Metabolic Changes in Radiation-associated IHD

Subjects: Endocrinology & Metabolism
Contributor: Nataša Anastasov

Label-free quantitative proteomics analysis showed that proteins involved in the lipid metabolism, sirtuin signaling, mitochondrial function, cytoskeletal organization, and antioxidant defense were the most affected. A histopathological analysis elucidated large foci of fibrotic tissue, myocardial lipomatosis and lymphocytic infiltrations in the irradiated samples. These data highlight the suitability of FFPE material for proteomics analysis. The study confirms the previous results emphasizing the role of adverse metabolic changes in the radiation-associated IHD. Most importantly, it excludes age at the time of death as a confounding factor.

Keywords: FFPE ; ionizing radiation ; occupational exposure ; proteomics ; label-free ; PPAR alpha ; heart ; ischemia ; cardiovascular disease

1. Introduction

Epidemiological studies in the Mayak Production Association occupationally exposed to chronic low-dose-rate radiation have shown a significant increase in the incidence of ischemic heart disease (IHD) causally associated with the total external gamma-ray dose. The association remains after correction for multiple competing factors such as smoking and alcohol consumption[1][2][3][4].

Previous proteomics study using fresh-frozen tissue obtained at autopsy from the cardiac left ventricle from Mayak workers showed a dose-dependent downregulation of proteins involved in mitochondrial energy metabolism, cardiac cytoskeleton, and oxidative stress response when compared to the samples from non-irradiated controls[5][6]. However, in this study, the individuals in the occupationally exposed group (>500 mGy) were on average 10 years older than the control subjects[5]. We applied a statistical method to distinguish the dose-only dependent protein expression changes from those of the age-only dependent changes. The analysis indicated that the majority of the proteins were deregulated by the radiation dose and not the age [6]. However, the confounding role of age could not be totally excluded. To address this issue, we initiated a new study where the control group was older than the irradiated group. Due to the difficulty of obtaining additional fresh-frozen material, we decided to use formalin-fixed, paraffin-embedded (FFPE) left ventricle tissue in the new study.

FFPE tissue is an ideal source of analytical material for clinical investigations due to its stability in long-term storage[7][8][9][10][11][12][13]. The technical improvement of proteome analysis using FFPE material is a prerequisite for the successful elucidation of biological pathways. However, in spite of several technical improvements, proteomic analysis using FFPE material as an alternative to fresh-frozen tissue remains a challenge [14][15][16][17][18][19][20][21]. The harsh conditions typically used for fixation have previously prohibited successful protein identification and reproducible protein quantification[18][19][22][23]. During the formalin fixation proteins undergo degradation and cross-linking. The fixation results in a 30 Da Hydroxymethyl modification, tagged mainly on lysine residues contributing to the inter- and intramolecular cross-linking reactions[19][22][24][25]. Lysine modification affects the efficiency of protein extraction and digestion[19][26][27]. The Mass Spectrometry analysis often showed a general preferential detection of tryptic peptides with the C-terminal arginine over lysine indicating that modified lysine residues are inaccessible to protease during digestion[19][26][27].

A variety of methods that have been developed allowing the extraction of proteins from FFPE samples[9][28][29][30] have proven to be quite successful in performing proteomics analysis[9][31]. However, only a few proteomics studies using human FFPE cardiac tissue exist, probably due to the lack of this type of biomaterial[32][33].

The data presented here show the compatibility of FFPE tissue for a proteomic approach. The study suggests that chronic radiation exposure induces alterations in the heart metabolism, structure and oxidative stress response that may contribute to the radiation-induced IHD. Furthermore, it shows that these alterations are not caused by normal ageing.

2. Proteomic Analysis of FFPE Cardiac Tissue Showed Alteration of the Heart Proteome after Chronic Irradiation

Among the quantified proteins with two or more unique peptides, the expression level of 196 proteins was significantly different between irradiated samples and controls (2 unique peptides; ±1.3-fold; $p < 0.05$). Of these, 105 proteins were downregulated and 91 upregulated in the irradiated samples (Table 1).

Table 1. Significantly deregulated proteins in irradiated cardiac left ventricle proteome. The proteins listed in the table were identified and quantified by two or more unique peptides; fold changes and *p*-values are shown.

Accession	ID	Annotation	Fold Changes	*p*-Value
P00746	CFD	Complement factor D	9.3	7.86×10^{-3}
Q96PD5	PGLYRP2	N-acetylmuramoyl-L-alanine amidase	7.7	9.62×10^{-3}
P04745	AMY1B	Amylase, alpha 1B	7.3	4×10^{-2}
Q96JB5	CDK5RAP3	CDK5 regulatory subunit-associated protein 3	6.3	3.31×10^{-4}
P34897	SHMT2	Serine hydroxymethyltransferase, mitochondrial	6.0	2.99×10^{-2}
Q9BQE5	APOL2	Apolipoprotein L2	5.8	3.82×10^{-5}
P20700	LMNB1	Lamin-B1	5.7	1.87×10^{-2}
P05452	CLEC3B	Tetranectin	5.6	4.23×10^{-2}
O60784	TOM1	Target of Myb protein 1	4.4	1.10×10^{-2}
Q6ICL3	TANGO2	Transport and golgi organization 2 homolog	3.7	2.41×10^{-2}
Q08209	PPP3CA	Serine/threonine-protein phosphatase 2B catalytic alpha	3.4	2.22×10^{-2}
P37802	TAGLN2	Transgelin-2	3.3	1.67×10^{-3}
Q01518	CAP1	Adenylyl cyclase-associated protein 1	3.3	1.84×10^{-5}
A0A0A0MS15	IGHV3-49	Immunoglobulin heavy variable 3-49	3.2	1.98×10^{-2}
P13591	NCAM1	Neural cell adhesion molecule 1	3.1	4.16×10^{-2}
O95336	PGLS	6-phosphogluconolactonase	3.1	3.25×10^{-2}
Q99715	COL12A1	Collagen alpha-1(XII) chain	3.1	2.22×10^{-2}
O95865	DDAH2	N(G),N(G)-dimethylarginine dimethylaminohydrolase 2	3.0	5.28×10^{-3}
Q5T0D9	TPRG1L	Tumor protein p63 regulated 1 like	3.0	3.05×10^{-4}
P31327	CPS1	Carbamoyl-phosphate synthase, mitochondrial	2.9	3.27×10^{-2}
P07738	BPGM	Bisphosphoglycerate mutase	2.9	1.28×10^{-2}
P61221	ABCE1	ATP-binding cassette sub-family E member 1	2.9	4.21×10^{-2}
Q7Z3Y8	KRT27	Keratin, type I cytoskeletal 27	2.7	4.64×10^{-3}
Q16610	ECM1	Extracellular matrix protein 1	2.7	3.03×10^{-2}
P05156	CFI	Complement factor I	2.7	1.41×10^{-2}
P01780	IGHV3-7	Immunoglobulin heavy variable 3-7	2.6	1.14×10^{-2}
P05546	SERPIND1	Heparin cofactor 2	2.6	5.00×10^{-2}
O75122	CLASP2	CLIP-associating protein 2	2.6	4.21×10^{-2}
Q2TAA2	IAH1	Isoamyl acetate-hydrolyzing esterase 1 homolog	2.5	3.13×10^{-2}
P16070	CD44	CD44 antigen	2.4	4.01×10^{-3}
P49721	PSMB2	Proteasome subunit beta type-2	2.4	6.87×10^{-7}
P13667	PDIA4	Protein disulfide-isomerase A4	2.4	6.55×10^{-3}

Accession	ID	Annotation	Fold Changes	*p*-Value
P35858	IGFALS	Insulin-like growth factor-binding protein complex acid labile	2.3	3.50×10^{-2}
P19652	ORM2	Alpha-1-acid glycoprotein 2	2.3	2.06×10^{-2}
O96007	MOCS2	Molybdopterin synthase catalytic subunit	2.3	8.91×10^{-4}
P08294	SOD3	Extracellular superoxide dismutase [Cu-Zn]	2.2	5.01×10^{-2}
Q6FI13	HIST2H2AA	Histone cluster 2 H2A family member a4	2.2	3.55×10^{-3}
P00488	F13A1	Coagulation factor XIII A chain	2.2	3.71×10^{-3}
P02649	APOE	Apolipoprotein E	2.2	3.95×10^{-2}
Q9HBI1	PARVB	Beta-parvin	2.2	1.49×10^{-2}
Q9BR76	CORO1B	Coronin-1B	2.1	1.26×10^{-2}
P28074	PSMB5	Proteasome subunit beta type-5	2.1	9.94×10^{-4}
P01714	IGLV3-19	Immunoglobulin lambda variable 3-19	2.0	1.91×10^{-2}
O60888	CUTA	Protein CutA	2.0	1.25×10^{-2}
Q16658	FSCN1	Fascin	2.0	3.42×10^{-2}
Q9ULV4	CORO1C	Coronin-1C	2.0	1.02×10^{-2}
P17655	CAPN2	Calpain-2 catalytic subunit	2.0	1.58×10^{-2}
Q15582	TGFBI	Transforming growth factor-beta-induced protein ig-h3	2.0	3.83×10^{-2}
P15144	ANPEP	Aminopeptidase N	1.9	3.32×10^{-2}
P01008	SERPINC1	Antithrombin-III	1.9	2.66×10^{-2}
Q96HY7	DHTKD1	Probable 2-oxoglutarate dehydrogenase E1 component	1.9	4.54×10^{-2}
P39059	COL15A1	Collagen alpha-1(XV) chain	1.8	3.28×10^{-2}
P35754	GLRX	Glutaredoxin-1	1.8	4.58×10^{-2}
P40121	CAPG	Macrophage-capping protein	1.8	2.32×10^{-2}
P36269	GGT5	Glutathione hydrolase 5 proenzyme	1.8	3.04×10^{-2}
O75340	PDCD6	Programmed cell death protein 6	1.8	9.00×10^{-3}
P12109	COL6A1	Collagen alpha-1(VI) chain	1.8	3.09×10^{-2}
P19827	ITIH1	Inter-alpha-trypsin inhibitor heavy chain H1	1.7	4.77×10^{-2}
P05109	S100A8	Protein S100-A8	1.7	3.47×10^{-2}
P36543	ATP6V1E1	V-type proton ATPase subunit E 1	1.7	1.10×10^{-2}
P04040	CAT	Catalase	1.7	2.98×10^{-2}
P12110	COL6A2	Collagen alpha-2(VI) chain	1.7	3.98×10^{-2}
P62191	PSMC1	26S proteasome regulatory subunit 4	1.7	3.55×10^{-2}
Q16647	PTGIS	Prostacyclin synthase	1.6	2.95×10^{-2}
Q9NZN3	EHD3	EH domain-containing protein 3	1.6	6.77×10^{-3}
Q9UJZ1	STOML2	Stomatin-like protein 2, mitochondrial	1.6	2.81×10^{-2}
P25786	PSMA1	Proteasome subunit alpha type-1	1.6	3.65×10^{-2}
Q8IUE6	HIST2H2AB	Histone H2A type 2-B	1.5	1.13×10^{-2}
Q13084	MRPL28	Mitochondrial ribosomal protein L28	1.5	5.01×10^{-2}
Q13162	PRDX4	Peroxiredoxin-4	1.5	3.24×10^{-2}

Accession	ID	Annotation	Fold Changes	*p*-Value
Q9Y490	TLN1	Talin-1	1.5	2.94×10^{-2}
Q15121	PEA15	Astrocytic phosphoprotein PEA-15	1.5	3.16×10^{-2}
Q9H4M9	EHD1	EH domain-containing protein 1	1.5	1.64×10^{-2}
O75396	SEC22B	Vesicle-trafficking protein SEC22b	1.5	7.62×10^{-3}
P24821	TNC	Tenascin	1.4	4.70×10^{-3}
P02766	TTR	Transthyretin	1.4	4.35×10^{-3}
P02042	HBD	Hemoglobin subunit delta	1.4	2.66×10^{-2}
P78527	PRKDC	DNA-dependent protein kinase catalytic subunit	1.4	4.48×10^{-2}
P25788	PSMA3	Proteasome subunit alpha type-3	1.4	4.59×10^{-2}
P68871	HBB	Hemoglobin subunit beta	1.4	1.54×10^{-2}
P07451	CA3	Carbonic anhydrase 3	1.4	4.69×10^{-2}
P26447	S100A4	S100 calcium binding protein A4	1.4	9.24×10^{-3}
P0C0S5	H2AFZ	Histone H2A.Z	1.4	1.23×10^{-2}
P51398	DAP3	28S ribosomal protein S29, mitochondrial	1.4	4.85×10^{-4}
P28072	PSMB6	Proteasome subunit beta type-6	1.4	3.67×10^{-2}
P23284	PPIB	Peptidyl-prolyl cis-trans isomerase B	1.4	2.32×10^{-2}
P04196	HRG	Histidine-rich glycoprotein	1.3	4.56×10^{-2}
Q14697	GANAB	Neutral alpha-glucosidase AB	1.3	4.40×10^{-2}
P00915	CA1	Carbonic anhydrase 1	1.3	1.55×10^{-2}
Q96QK1	VPS35	Vacuolar protein sorting-associated protein 35	1.3	2.98×10^{-2}
P69905	HBA2	Hemoglobin subunit alpha 2	1.3	3.55×10^{-2}
P35613	BSG	Basigin	0.76	7.53×10^{-3}
P51649	ALDH5A1	Succinate-semialdehyde dehydrogenase, mitochondrial	0.76	2.80×10^{-2}
P62263	RPS14	Ribosomal protein S14	0.76	4.03×10^{-2}
P09429	HMGB1	High mobility group protein B1	0.76	5.01×10^{-2}
Q9H7Z7	PTGES2	Prostaglandin E synthase 2	0.76	3.68×10^{-2}
Q9Y2Z9	COQ6	Ubiquinone biosynthesis monooxygenase COQ6	0.75	1.62×10^{-2}
Q8NDY3	ADPRHL1	[Protein ADP-ribosylarginine] hydrolase-like protein 1	0.75	4.76×10^{-2}
Q7Z406	MYH14	Myosin-14	0.75	4.69×10^{-2}
Q16698	DECR1	2,4-dienoyl-CoA reductase, mitochondrial	0.75	4.16×10^{-2}
Q03252	LMNB2	Lamin-B2	0.75	8.66×10^{-3}
P10916	MYL2	Myosin regulatory light chain 2, ventricular/cardiac	0.75	2.03×10^{-2}
Q0ZGT2	NEXN	Nexilin	0.74	4.74×10^{-2}
E7EW31	PROB1	Proline rich basic protein 1	0.74	4.33×10^{-2}
P52179	MYOM1	Myomesin-1	0.73	8.85×10^{-3}
Q9Y265	RUVBL1	RuvB-like 1	0.73	3.98×10^{-2}
P46777	RPL5	60S ribosomal protein L5	0.73	3.86×10^{-3}
P30038	ALDH4A1	Delta-1-pyrroline-5-carboxylate dehydrogenase	0.73	2.60×10^{-2}

Accession	ID	Annotation	Fold Changes	*p*-Value
P32119	PRDX2	Peroxiredoxin-2	0.73	2.77×10^{-2}
P45379	TNNT2	Troponin T, cardiac muscle	0.73	8.78×10^{-3}
O75521	ECI2	Enoyl-CoA delta isomerase 2, mitochondrial	0.72	4.43×10^{-2}
Q16836	HADH	Hydroxyacyl-coenzyme A dehydrogenase, mitochondrial	0.72	1.58×10^{-2}
Q9BTZ2	DHRS4	Dehydrogenase/reductase SDR family member 4	0.72	1.67×10^{-2}
P07339	CTSD	Cathepsin D	0.72	1.31×10^{-3}
Q9BX66	SORBS1	Sorbin and SH3 domain-containing protein 1	0.72	3.43×10^{-2}
Q15046	KARS	Lysine—tRNA ligase	0.71	2.49×10^{-2}
O75438	NDUFB1	NADH dehydrogenase [ubiquinone] 1 beta subcomplex 1	0.71	1.62×10^{-2}
O95817	BAG3	BAG family molecular chaperone regulator 3	0.71	3.99×10^{-2}
Q9UL25	RAB21	Ras-related protein Rab-21	0.71	3.92×10^{-2}
P21397	MAOA	Amine oxidase [flavin-containing] A	0.70	7.04×10^{-3}
Q96HS1	PGAM5	Serine/threonine-protein phosphatase PGAM5	0.70	1.43×10^{-2}
Q9Y5J7	TIMM9	Mitochondrial import inner membrane translocase	0.70	1.36×10^{-2}
O75947	ATP5H	ATP synthase subunit d, mitochondrial	0.70	2.39×10^{-2}
P19429	TNNI3	Troponin I, cardiac muscle	0.69	9.61×10^{-3}
P62753	RPS6	40S ribosomal protein S6	0.69	2.02×10^{-2}
Q13045	FLII	Protein flightless-1 homolog	0.69	1.78×10^{-2}
O95292	VAPB	Vesicle-associated membrane protein-associated protein	0.68	1.72×10^{-2}
P02511	CRYAB	Alpha-crystallin B chain	0.67	3.99×10^{-3}
P15121	AKR1B1	Aldose reductase	0.67	5.01×10^{-2}
Q9NUJ1	ABHD10	Mycophenolic acid acyl-glucuronide esterase	0.67	1.49×10^{-3}
P46779	RPL28	60S ribosomal protein L28	0.67	3.76×10^{-2}
Q6PIU2	NCEH1	Neutral cholesterol ester hydrolase 1	0.67	4.07×10^{-2}
Q8WWI1	LMO7	LIM domain only protein 7	0.66	5.01×10^{-2}
Q9UFN0	NIPSNAPA	Nipsnap homolog 3A	0.66	2.13×10^{-3}
Q14118	DAG1	Dystroglycan	0.66	7.65×10^{-3}
Q5BKX8	MURC	Caveolae-associated protein 4	0.65	1.78×10^{-3}
Q6IAA8	LAMTOR1	Ragulator complex protein LAMTOR1	0.65	2.14×10^{-2}
O43676	NDUFB3	NADH dehydrogenase [ubiquinone] 1 beta subcomplex 3	0.65	3.38×10^{-2}
P49368	CCT3	T-complex protein 1 subunit gamma	0.64	1.01×10^{-2}
P63220	RPS21	Ribosomal protein S21	0.64	1.14×10^{-2}
Q9UMR2	DDX19B	ATP-dependent RNA helicase DDX19B	0.64	5.87×10^{-5}
Q8NBN7	RDH13	Retinol dehydrogenase 13	0.64	4.74×10^{-2}
Q14192	FHL2	Four and a half LIM domains protein 2	0.64	5.01×10^{-2}
O76024	WFS1	Wolframin	0.64	4.83×10^{-2}
P30084	ECHS1	Enoyl-CoA hydratase, mitochondrial	0.63	5.17×10^{-3}
Q9HBL7	PLGRKT	Plasminogen receptor (KT)	0.63	2.44×10^{-2}

Accession	ID	Annotation	Fold Changes	*p*-Value
P26440	IVD	Isovaleryl-CoA dehydrogenase, mitochondrial	0.63	2.67×10^{-2}
P60866	RPS20	Ribosomal protein S20	0.62	3.18×10^{-2}
Q6DN03	HIST2H2BC	Putative histone H2B type 2-C	0.62	1.71×10^{-2}
Q99460	PSMD1	26S proteasome non-ATPase regulatory subunit 1	0.61	1.71×10^{-2}
Q96PE7	MCEE	Methylmalonyl-CoA epimerase, mitochondrial	0.61	1.44×10^{-2}
Q8N3J5	PPM1K	Protein phosphatase 1K, mitochondrial	0.61	2.98×10^{-2}
Q9Y5K5	UCHL5	Ubiquitin carboxyl-terminal hydrolase isozyme L5	0.61	1.82×10^{-4}
Q9H987	SYNPO2L	Synaptopodin 2-like protein	0.60	2.82×10^{-2}
O95182	NDUFA7	NADH dehydrogenase [ubiquinone] 1 alpha 7	0.59	8.36×10^{-3}
Q9NQR4	NIT2	Omega-amidase NIT2	0.59	1.48×10^{-2}
Q96ND0	FAM210A	Protein FAM210A	0.58	3.74×10^{-2}
P46109	CRKL	Crk-like protein	0.58	2.56×10^{-2}
Q13409	DYNC1I2	Cytoplasmic dynein 1 intermediate chain 2	0.57	9.61×10^{-3}
P62906	RPL10A	60S ribosomal protein L10a	0.57	1.81×10^{-2}
Q8NF91	SYNE1	Nesprin-1	0.57	2.02×10^{-2}
O94875	SORBS2	Sorbin and SH3 domain-containing protein 2	0.56	2.55×10^{-2}
Q9BS92	NIPSNAP3B	Nipsnap homolog 3B	0.56	5.01×10^{-2}
Q13151	HNRNPA0	Heterogeneous nuclear ribonucleoprotein A0	0.55	1.94×10^{-2}
P82675	MRPS5	Mitochondrial ribosomal protein S5	0.55	1.17×10^{-2}
P22830	FECH	Ferrochelatase, mitochondrial	0.55	9.32×10^{-3}
Q5HYJ1	TECRL	trans-2,3-enoyl-CoA reductase like	0.55	4.59×10^{-3}
Q9Y285	FARSA	phenylalanyl-tRNA synthetase alpha subunit	0.54	2.10×10^{-4}
Q8TB22	SPATA20	Spermatogenesis-associated protein 20	0.53	4.46×10^{-3}
Q9NP72	RAB18	Ras-related protein Rab-18	0.52	4.87×10^{-3}
O75190	DNAJB6	DnaJ homolog subfamily B member 6	0.52	8.53×10^{-3}
P35542	SAA4	Serum amyloid A-4 protein	0.51	3.04×10^{-2}
E9PAV3	NACA	Nascent polypeptide-associated complex subunit alpha	0.49	5.23×10^{-5}
Q8N6M3	FITM2	Fat storage-inducing transmembrane protein 2	0.48	1.85×10^{-2}
P27816	MAP4	Microtubule-associated protein 4	0.47	4.48×10^{-2}
P0CAP1	MYZAP	Myocardial zonula adherens protein	0.47	1.87×10^{-2}
Q96AB3	ISOC2	Isochorismatase domain containing 2	0.46	9.70×10^{-3}
Q562R1	ACTBL2	Beta-actin-like protein 2	0.44	3.63×10^{-2}
Q9NS69	TOMM22	Mitochondrial import receptor subunit TOM22 homolog	0.43	1.34×10^{-2}
Q9BXK5	BCL2L13	Bcl-2-like protein 13	0.42	2.93×10^{-2}
Q16543	CDC37	Hsp90 co-chaperone Cdc37	0.42	5.00×10^{-2}
P43155	CRAT	Carnitine O-acetyltransferase	0.42	1.24×10^{-3}
Q5VWP3	MLIP	Muscular LMNA-interacting protein	0.41	3.38×10^{-2}
O60488	ACSL4	Long-chain-fatty-acid—CoA ligase 4	0.40	2.89×10^{-4}

Accession	ID	Annotation	Fold Changes	*p*-Value
Q08722	CD47	Leukocyte surface antigen CD47	0.39	6.97×10^{-3}
Q6Y288	B3GALTL	Beta-1,3-glucosyltransferase	0.38	4.29×10^{-3}
P43487	RANBP1	Ran-specific GTPase-activating protein	0.35	1.93×10^{-6}
P01040	CSTA	Cystatin-A	0.33	3.50×10^{-2}
P48506	GCLC	Glutamate—cysteine ligase catalytic subunit	0.33	4.30×10^{-2}
P08621	SNRNP70	U1 small nuclear ribonucleoprotein 70 kDa	0.30	2.09×10^{-3}
P23919	DTYMK	Thymidylate kinase	0.30	6.33×10^{-3}
O95394	PGM3	Phosphoacetylglucosamine mutase	0.29	4.82×10^{-2}
P12829	MYL4	Myosin light chain 4	0.26	2.84×10^{-4}
Q9NX40	OCIAD1	OCIA domain-containing protein 1	0.19	1.96×10^{-3}
Q08830	FGL1	Fibrinogen-like protein 1	0.12	4.76×10^{-3}
Q08397	LOXL1	Lysyl oxidase homolog 1	0.08	2.20×10^{-2}

A volcano plot of all quantified and significantly deregulated proteins is shown in Figure 1A. The heat map based on the intensity of differentially regulated proteins in all individual samples showed a clear difference between the control and irradiated groups (Figure 1B).

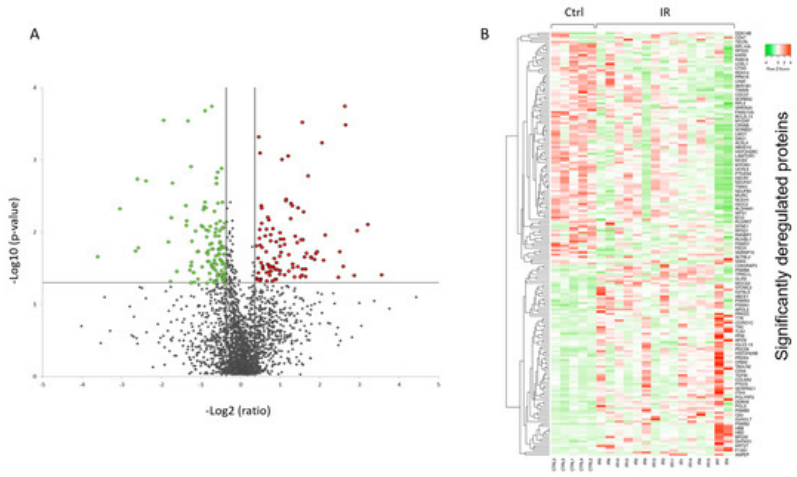

Figure 1. Graphical representation of quantitative proteomics data of human FFPE cardiac tissue after chronic irradiation. Proteins are ranked in a volcano plot according to the −log10 of their statistical *p*-value (y-axis) and log2 fold change (x-axis). The green and red points represent the significantly downregulated and upregulated proteins, respectively (**A**). The heat map shows hierarchical clustering (average linkage, Spearman ranked correlation) of significantly deregulated proteins in 5 controls (Ctrl) and 15 irradiated (IR) samples (**B**). The green bars indicate downregulation and the red bars upregulation. The analysis was performed using Heatmapper web server.

Among the differentially regulated proteins were several lipid metabolism enzymes (Table 1). Long-chain-fatty-acid—CoA ligase 4 (ACSL4), hydroxyacyl-coenzyme A dehydrogenase (HADH), 2,4-dienoyl-CoA reductase (DECR1), enoyl-CoA hydratase (ECHS1), isovaleryl-CoA dehydrogenase (IVD), and enoyl-CoA delta isomerase 2 (ECI2) were all downregulated.

A number of proteins belonging to the sirtuin pathway and mitochondrial respiratory chain were also significantly downregulated in the irradiated samples (Table 1). The level of mitochondrial import inner membrane translocase (TIMM9), mitochondrial import receptor (TOMM22), and that of several proteins in the mitochondrial complexes I and V was reduced in the irradiated samples (Table 1).

Similarly, the data also showed downregulation in the expression of actin cytoskeleton components such as troponin I (TNNI3), troponin T (TNNT2), and different myosin isoforms including myosin heavy chain 14 (MYH14), myosin regulatory light chain 2 (MYL2), myosin light chain 4 (MYL4), and myomesin-1 (MYOM1) (Table 1). In contrast, several collagen

isoforms were upregulated in the proteomics data, including collagen type XII alpha 1 chain (COL12A1), collagen type XV alpha 1 chain (COL15A), collagen type VI alpha 1 chain (COL6A) and collagen type VI alpha 2 chain (COL6A2) (Table 1).

The levels of several proteins of the oxidative stress response, namely catalase (CAT), peroxiredoxin 2 (PRDX2), peroxiredoxin 4 (PRDX4), extracellular superoxide dismutase [Cu-Zn] (SOD3), glutathione hydrolase 5 (GGT5), and glutaredoxin-1 (GLRX), were altered, most showing upregulation (Table 1).

A detailed analysis of the functional interactions and biological pathways of the deregulated proteins was performed using Ingenuity Pathway Analysis (IPA) software. Fatty acid metabolism, sirtuin signaling, mitochondrial dysfunction, protein ubiquitination, tissue fibrosis, cytoskeleton organization, and oxidative stress were the most affected pathways in the irradiated samples compared to the control (Figure 2A). Especially two biological networks showed enrichment of deregulated proteins. The predicted regulators of these networks were the peroxisome proliferator-activated receptor (PPAR) alpha and transforming growth factor beta-1 (TGFB1) (Figure 2B,C). PPAR alpha was predicted to be inactivated in irradiated samples, whilst TGF beta was predicted to be activated. Differentially expressed proteins were associated with cardiotoxicity-related pathways including cardiac dilation, cardiac enlargement, cardiac dysfunction, heart failure, and cardiac fibrosis.

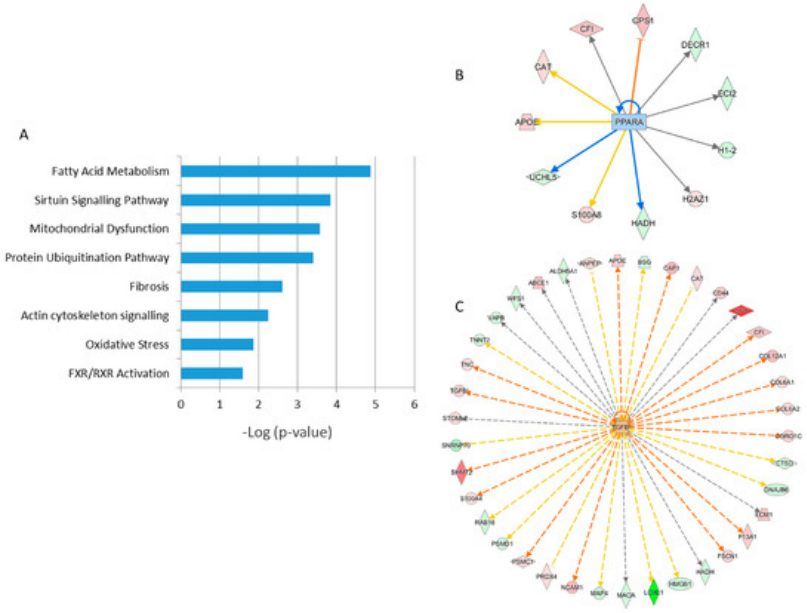

Figure 2. Pathway analysis of differentially regulated proteins from human FFPE heart tissues. The most significant canonical pathways altered by irradiation are shown. The analyses were generated using Ingenuity Pathway Analysis (IPA) (QIAGEN Inc., Hilden, Germany). The bars indicate canonical pathways and the y-axis displays the −(log *p*) enrichment significance. The tall bars are more significant than the short ones (**A**). Graphical representation of the deregulated protein networks with their upstream transcriptional regulators peroxisome proliferator-activated receptor (PPAR) alpha (**B**) and transforming growth factor beta (TGFB) (**C**) are shown. The upregulated proteins are marked in red and the downregulated in green. The nodes in blue (inhibition) and orange (activation) represent transcription factors. The full protein names are given in Table 1.

References

1. Azizova, T.V.; Grigorieva, E.S.; Hunter, N.; Pikulina, M.V.; Moseeva, M.B. Risk of mortality from circulatory diseases in Mayak workers cohort following occupational radiation exposure. J. Radiol. Prot. 2015, 35, 517–538.
2. Azizova, T.V.; Muirhead, C.R.; Druzhinina, M.B.; Grigoryeva, E.S.; Vlasenko, E.V.; Sumina, M.V.; O'Hagan, J.A.; Zhang, W.; Haylock, R.G.; Hunter, N. Cardiovascular diseases in the cohort of workers first employed at Mayak PA in 1948–1958. Radiat. Res. 2010, 174, 155–168.
3. Azizova, T.V.; Muirhead, C.R.; Moseeva, M.B.; Grigoryeva, E.S.; Vlasenko, E.V.; Hunter, N.; Haylock, R.G.; O'Hagan, J.A. Ischemic heart disease in nuclear workers first employed at the Mayak PA in 1948–1972. Health Phys. 2012, 103, 3–14.
4. Azizova, T.V.; Grigoryeva, E.S.; Haylock, R.G.; Pikulina, M.V.; Moseeva, M.B. Ischaemic heart disease incidence and mortality in an extended cohort of Mayak workers first employed in 1948–1982. Br. J. Radiol. 2015, 88, 20150169.
5. Azimzadeh, O.; Azizova, T.; Merl-Pham, J.; Subramanian, V.; Bakshi, M.V.; Moseeva, M.; Zubkova, O.; Hauck, S.M.; Anastasov, N.; Atkinson, M.J.; et al. A dose-dependent perturbation in cardiac energy metabolism is linked to radiation-

induced ischemic heart disease in Mayak nuclear workers. Oncotarget 2017, 8, 9067–9078.

6. Papiez, A.; Azimzadeh, O.; Azizova, T.; Moseeva, M.; Anastasov, N.; Smida, J.; Tapio, S.; Polanska, J. Integrative multiomics study for validation of mechanisms in radiation-induced ischemic heart disease in Mayak workers. PLoS ONE 2018, 13, e0209626.
7. Bayer, M.; Angenendt, L.; Schliemann, C.; Hartmann, W.; Konig, S. Are formalin-fixed and paraffin-embedded tissues fit for proteomic analysis? J. Mass Spectrom. 2019, 55, e4347.
8. Zhu, Y.; Weiss, T.; Zhang, Q.; Sun, R.; Wang, B.; Yi, X.; Wu, Z.; Gao, H.; Cai, X.; Ruan, G.; et al. High-throughput proteomic analysis of FFPE tissue samples facilitates tumor stratification. Mol. Oncol. 2019, 13, 2305–2328.
9. Giusti, L.; Angeloni, C.; Lucacchini, A. Update on proteomic studies of formalin-fixed paraffin-embedded tissues. Expert Rev. Proteom. 2019, 16, 513–520.
10. Tapio, S.; Hornhardt, S.; Gomolka, M.; Leszczynski, D.; Posch, A.; Thalhammer, S.; Atkinson, M.J. Use of proteomics in radiobiological research: Current state of the art. Radiat. Environ. Biophys. 2010, 49, 1–4.
11. Tapio, S.; Atkinson, M.J. Molecular information obtained from radiobiological tissue archives: Achievements of the past and visions of the future. Radiat. Environ. Biophys. 2008, 47, 183–187.
12. Tapio, S.; Schofield, P.N.; Adelmann, C.; Atkinson, M.J.; Bard, J.L.; Bijwaard, H.; Birschwilks, M.; Dubus, P.; Fiette, L.; Gerber, G.; et al. Progress in updating the European Radiobiology Archives. Int. J. Radiat. Biol. 2008, 84, 930–936.
13. Gustafsson, O.J.; Arentz, G.; Hoffmann, P. Proteomic developments in the analysis of formalin-fixed tissue. Biochim. Biophys. Acta 2015, 1854, 559–580.
14. Nirmalan, N.J.; Harnden, P.; Selby, P.J.; Banks, R.E. Development and validation of a novel protein extraction methodology for quantitation of protein expression in formalin-fixed paraffin-embedded tissues using western blotting. J. Pathol. 2009, 217, 497–506.
15. Tanca, A.; Addis, M.F.; Pagnozzi, D.; Cossu-Rocca, P.; Tonelli, R.; Falchi, G.; Eccher, A.; Roggio, T.; Fanciulli, G.; Uzzau, S. Proteomic analysis of formalin-fixed, paraffin-embedded lung neuroendocrine tumor samples from hospital archives. J. Proteom. 2011, 74, 359–370.
16. Azimzadeh, O.; Scherthan, H.; Yentrapalli, R.; Barjaktarovic, Z.; Ueffing, M.; Conrad, M.; Neff, F.; Calzada-Wack, J.; Aubele, M.; Buske, C.; et al. Label-free protein profiling of formalin-fixed paraffin-embedded (FFPE) heart tissue reveals immediate mitochondrial impairment after ionising radiation. J. Proteom. 2012, 75, 2384–2395.
17. Tanca, A.; Pagnozzi, D.; Burrai, G.P.; Polinas, M.; Uzzau, S.; Antuofermo, E.; Addis, M.F. Comparability of differential proteomics data generated from paired archival fresh-frozen and formalin-fixed samples by GeLC-MS/MS and spectral counting. J. Proteom. 2012, 77, 561–576.
18. Giusti, L.; Lucacchini, A. Proteomic studies of formalin-fixed paraffin-embedded tissues. Expert Rev. Proteom. 2013, 10, 165–177.
19. Azimzadeh, O.; Barjaktarovic, Z.; Aubele, M.; Calzada-Wack, J.; Sarioglu, H.; Atkinson, M.J.; Tapio, S. Formalin-fixed paraffin-embedded (FFPE) proteome analysis using gel-free and gel-based proteomics. J. Proteome Res. 2010, 9, 4710–4720.
20. Wisniewski, J.R.; Dus, K.; Mann, M. Proteomic workflow for analysis of archival formalin-fixed and paraffin-embedded clinical samples to a depth of 10000 proteins. Proteom. Clin. Appl. 2013, 7, 225–233. [Google Scholar] [CrossRef]
21. Wisniewski, J.R.; Zougman, A.; Nagaraj, N.; Mann, M. Universal sample preparation method for proteome analysis. Nat. Methods 2009, 6, 359–362.
22. Metz, B.; Kersten, G.F.; Hoogerhout, P.; Brugghe, H.F.; Timmermans, H.A.; de Jong, A.; Meiring, H.; ten Hove, J.; Hennink, W.E.; Crommelin, D.J.; et al. Identification of formaldehyde-induced modifications in proteins: Reactions with model peptides. J. Biol. Chem. 2004, 279, 6235–6243.
23. Steiner, C.; Ducret, A.; Tille, J.C.; Thomas, M.; McKee, T.A.; Rubbia-Brandt, L.; Scherl, A.; Lescuyer, P.; Cutler, P. Applications of mass spectrometry for quantitative protein analysis in formalin-fixed paraffin-embedded tissues. Proteomics 2014, 14, 441–451.
24. Fowler, C.B.; Cunningham, R.E.; O'Leary, T.J.; Mason, J.T. 'Tissue surrogates' as a model for archival formalin-fixed paraffin-embedded tissues. Lab. Investig. 2007, 87, 836–846.
25. Nirmalan, N.J.; Harnden, P.; Selby, P.J.; Banks, R.E. Mining the archival formalin-fixed paraffin-embedded tissue proteome: Opportunities and challenges. Mol. Biosyst. 2008, 4, 712–720.
26. Jiang, X.; Jiang, X.; Feng, S.; Tian, R.; Ye, M.; Zou, H. Development of efficient protein extraction methods for shotgun proteome analysis of formalin-fixed tissues. J. Proteome Res. 2007, 6, 1038–1047.

27. Sprung, R.W., Jr.; Brock, J.W.; Tanksley, J.P.; Li, M.; Washington, M.K.; Slebos, R.J.; Liebler, D.C. Equivalence of protein inventories obtained from formalin-fixed paraffin-embedded and frozen tissue in multidimensional liquid chromatography-tandem mass spectrometry shotgun proteomic analysis. Mol. Cell. Proteom. 2009, 8, 1988–1998.
28. Azimzadeh, O.; Atkinson, M.J.; Tapio, S. Qualitative and quantitative proteomic analysis of formalin-fixed paraffin-embedded (FFPE) tissue. Methods Mol. Biol. 2015, 1295, 109–115.
29. Foll, M.C.; Fahrner, M.; Oria, V.O.; Kuhs, M.; Biniossek, M.L.; Werner, M.; Bronsert, P.; Schilling, O. Reproducible proteomics sample preparation for single FFPE tissue slices using acid-labile surfactant and direct trypsinization. Clin. Proteom. 2018, 15, 1
30. Quesada-Calvo, F.; Bertrand, V.; Longuespee, R.; Delga, A.; Mazzucchelli, G.; Smargiasso, N.; Baiwir, D.; Delvenne, P.; Malaise, M.; De Pauw-Gillet, M.C.; et al. Comparison of two FFPE preparation methods using label-free shotgun proteomics: Application to tissues of diverticulitis patients. J. Proteom. 2015, 112, 250–261.
31. Gaffney, E.F.; Riegman, P.H.; Grizzle, W.E.; Watson, P.H. Factors that drive the increasing use of FFPE tissue in basic and translational cancer research. Biotech. Histochem. 2018, 93, 373–386.
32. Kakimoto, Y.; Ito, S.; Abiru, H.; Kotani, H.; Ozeki, M.; Tamaki, K.; Tsuruyama, T. Sorbin and SH3 domain-containing protein 2 is released from infarcted heart in the very early phase: Proteomic analysis of cardiac tissues from patients. J. Am. Heart Assoc. 2013, 2, e000565.
33. Holub, D.; Flodrova, P.; Pika, T.; Flodr, P.; Hajduch, M.; Dzubak, P. Mass Spectrometry Amyloid Typing Is Reproducible across Multiple Organ Sites. BioMed Res. Int. 2019, 2019, 3689091.